International Journal of Applied Electromagnetics in Materials 3 (1993) 297–306
Elsevier

Electromagnetic field source searching from the local field measurement

H. Saotome, K. Kitsuta, S. Hayano and Y. Saito

College of Engineering, Hosei University, Kajino, Koganei, Tokyo 184, Japan

Received 24 April 1992

First, we make a brief review of inverse problems in various fields and formulate the inverse problems in the electrostatic, magnetostatic and current flowing fields. Secondly, we propose one of the methods for obtaining a unique solution pattern, not a unique solution of the inverse problem. Finally, we apply our method to human heart diagnosis and current flow estimation in a human brain. As a result, the positions of defects in hearts exhibiting the Wolff–Parkinson–White syndrome are successfully identified and sequential current flows in a human brain are clarified by our approach.

1. Introduction

In 1917, Radon gave a mathematical background of computed tomography. After Oldendorf's experiment (1961) and Kuhl's experiment (1963), Hounsfield and Anbrose succeeded in realizing computed tomography [1]. Computed tomography could be one of the inverse problems in a broad sense and called the weakly ill-conditioned inverse problem, because available data are a set of orthogonal data around a target region. The essential inverse problem in medicine is the electromagnetic field source identification from the electrocardiogram (ECG), magnetocardiogram (MCG), electroencephalogram (EEG), magnetoencephalogram (MEG) and other electromagnetic data, which are insufficient to identify or find the field source distribution and field source amplitudes exactly.

In the electromagnetic field source searching problems, the difficulty of the inverse problems exists in the fact that the area of the known field does not include the source existing region. In other words, if the field measurement region include the source existing positions, the source can be easily obtained by spatially differentiating the field. In this case, the governing equation has a differential form. However, the governing equation becomes an integral form in the inverse problem because of the lack of field information.

In the present paper, we propose a method for obtaining a unique solution pattern, not a unique solution of the inverse problem. No unique solution can be usually expected in the inverse problems because the system matrix, obtained by discretizing the integral equation, is not a regular matrix.

Our proposed method is applied to human heart diagnosis and current flow estimation in a human brain. As a result, the positions of defect exhibiting the Wolff–Parkinson–White syndrome are successfully identified. Also, the current flow in a human brain is estimated when the median nerve of a right wrist is stimulated electrically.

Correspondence to: Dr. H. Saotome, College of Engineering, Hosei University, Kajino, Koganei, Tokyo 184, Japan.

2. Formulation of open boundary inverse problems

2.1. Electromagnetic field problems

In electrostatic fields, the electric potential ϕ is related with the charge density ρ and the

permittivity of free space ε_0 by

$$\varepsilon_0 \nabla^2 \phi = -\rho \,. \tag{1}$$

When we denote A as a vector potential, then the magnetostatic field problems are reduced to solving the following equation assuming the Coulomb gauge $\nabla \cdot A = 0$:

$$(1/\mu_0)\nabla^2 A = -J \,, \tag{2}$$

where μ_0 and J are the permeability of free space and current density, respectively.

In current flowing fields, the electric field intensity E is related with the electric potential ϕ by

$$E = -\nabla\phi \tag{3a}$$

and has the following relation:

$$J = \kappa E + J_s \,, \tag{3b}$$

where κ and J_s are the conductivity and current density springing out in conductive space, respectively. Substituting (3a) into (3b) and taking the divergence of (3b), we have

$$\kappa \nabla^2 \phi = \nabla \cdot J_s \,, \tag{4}$$

because of the relation $\nabla \cdot J = 0$.

Equations (1), (2) and (4) can be written generally in the form

$$\lambda \nabla^2 \psi = -\sigma \,, \tag{5}$$

where ψ, σ and λ are the scalar or vector potential, field source density and medium parameter, respectively.

The problem, in which the field source density σ and the medium parameter λ in entire space are given and the potential ψ is the unknown, is called a *forward* problem. A number of analytical studies in engineering and science have developed methodologies for solving this kind of problem. Also, most of the present numerical methods have been developed to solve this type of problem. On the other hand, obtaining the field source density σ using the potential ψ or field intensity as well as the medium parameter λ in entire space is called a *dual* problem.

In source searching problems, when the only local potential ψ in limited space not including the source existing region is given, the evaluation of the field source density σ is called an *inverse* problem. Stokes, Neuman and others already have pointed out that the lack of field or potential information results in ambiguity of the solution of the inverse problem [1].

2.2. Governing equations for inverse problems of electromagnetic fields

In the homogeneous medium cases, imposing the open boundary condition, the potential ψ in (5) is formally obtained by an integral form:

$$\psi = \int_V (G/\lambda)\sigma \, dv \,, \tag{6}$$

where G is the Green's function given by $G = 1/(4\pi r)$ in three-dimensional cases, and r is the distance between the potential and source points.

In the electrostatic fields, (6) becomes

$$\phi = \int_V [\rho/(4\pi\varepsilon_0 r)] \, dv \,. \tag{7}$$

Similarly, in the magnetostatic fields, (6) is

$$A = \mu_0 \int_V [J/(4\pi r)] \, dv \,, \tag{8a}$$

or

$$H = B/\mu_0 = \nabla \times \int_V [J/(4\pi r)] \, dv \,, \tag{8b}$$

where the magnetic field intensity $H = (1/\mu_0)\nabla \times A$. Further in the current flowing fields, (6) is

$$\phi = -\int_V [\nabla \cdot J_s/(4\pi\kappa r)] \, dv \,. \tag{9}$$

In the magnetostatic fields, the governing equation is not expressed by the vector potential, because it is difficult to measure the vector potential A directly.

2.3. System equations for inverse problems of electromagnetic fields

Discretizing in (6) into small subdivisions ΔV_i ($i = 1, 2, \ldots, m$) yields a system equation of the inverse problems:

$$U = \sum_{i=1}^{m} \alpha_i d_i , \tag{10}$$

where

$$U = [\psi_1, \psi_2, \ldots, \psi_n]^T , \tag{11}$$

$$d_i = [G_{1i}, G_{2i}, \ldots, G_{ni}]^T , \tag{12}$$

$$\alpha_i = (\sigma_i/\lambda)\, \Delta V_i . \tag{13}$$

In (11) and (12), the subscript n denotes the number of measured potential or field points. Generally, the number of source points m is much larger than the limited number of potential or field measured points n, thereby the following condition is established:

$$m \gg n . \tag{14}$$

In (12), the elements $G_{1i}, G_{2i}, \ldots, G_{ni}$ are the functions of the angles as well as distances between the field and source points. In (13), the unknown α_i, becomes a *voltage dipole* in the electrostatic and current flowing fields, but it becomes a *current dipole* in the magnetostatic fields, respectively.

In the electrostatic and current flowing fields, (11) and (12) are

$$U = [\phi_1, \phi_2, \ldots, \phi_n]^T , \tag{15}$$

$$d_i = \{1/(4\pi)\}[\boldsymbol{n}_i \cdot \boldsymbol{a}_{1i}/r_{1i}, \boldsymbol{n}_i \cdot \boldsymbol{a}_{2i}/r_{2i}, \ldots, \boldsymbol{n}_i \cdot \boldsymbol{a}_{ni}/r_{ni}]^T , \tag{16}$$

where $\boldsymbol{n}_i$ is unit space vector in the direction of the voltage dipoles. In the electrostatic fields,

$$\alpha_i = (\rho_i/\varepsilon_0)\, \Delta V_i , \tag{17}$$

and in the current flowing fields,

$$\alpha_i = (-\nabla \cdot \boldsymbol{J}_{si}/\kappa)\, \Delta V_i = -I_{si}/\kappa . \tag{18}$$

The current $\boldsymbol{I}_{si}$ in (18) springs from the surface of the volume ΔV_i, therefore, the absolute value of $\boldsymbol{I}_{si}$ is given by

$$I_{si} = |\boldsymbol{I}_{si}| = \int_{\Delta Vi} \nabla \cdot \boldsymbol{J}_{si}\, \mathrm{d}v = \int_{\Delta si} \boldsymbol{J}_{si} \cdot \mathrm{d}\boldsymbol{S} . \tag{19}$$

Moreover, $\boldsymbol{a}_{1i}, \boldsymbol{a}_{2i}, \ldots, \boldsymbol{a}_{ni}$ are unit space vectors from the source point i to the field points 1, 2, ..., n; and $r_{1i}, r_{2i}, \ldots, r_{ni}$ denote the distances between the source point i and the field points 1, 2, ..., n, respectively.

In the magnetostatic fields, (11) and (12) are

$$U = [\boldsymbol{H}_1, \boldsymbol{H}_2, \ldots, \boldsymbol{H}_n]^T , \tag{20}$$

$$d_i = [1/(4\pi)][\boldsymbol{n}_i \times \boldsymbol{a}_{1i}/r_{1i}^2, \boldsymbol{n}_i \times \boldsymbol{a}_{2i}/r_{2i}^2, \ldots, \boldsymbol{n}_i \times \boldsymbol{a}_{ni}/r_{ni}^2]^T , \tag{21}$$

where $\boldsymbol{n}_i$ is unit space vector in the direction of the current dipole $\boldsymbol{J}_i\, \Delta V_i$ assuming a constant current density $\boldsymbol{J}_i$ in a small subdivision ΔV_i [2–4]. Therefore, α_i in (10) can be written by

$$\alpha_i = |\boldsymbol{J}_i|\, \Delta V_i . \tag{22}$$

3. Unique solution pattern searching

Because the field or potential measurement area is not located in the source existing region in the inverse problem, it is obviously difficult to obtain a unique solution of (10). The condition (14) makes it mathematically difficult to solve (10). Namely, the number of equations n is much smaller than the number of the unknowns m. When $m \leqslant n$, we could have a square system matrix by using, for example, the Gram–Schmidt method, the factor analysis and so forth [5, 6]. However, even if the condition $n = m$ is held, solving (10) is still difficult because the determinant of the obtained system matrix becomes nearly zero. Also, the analysis using least squares gives the most dominant source position and its amplitude, but cannot provide plural source positions [4].

Therefore, we have developed a unique solution pattern searching algorithm called the *sampled pattern matching* (SPM) method [7–11]. The validity of the method has been examined by comparing the obtained source distribution pattern with the original one, because the comparison between the field patterns due to the original and estimated sources does not make sense in the inverse problem. The uniqueness of the source distribution patterns will be demonstrated in section 4.1.

It is possible to modify (10) into

$$U = \sum_{i=1}^{m} \left(\beta_i \boldsymbol{d}_i + \sum_{j \neq i}^{m} \left(\beta_{ij} (\boldsymbol{d}_i + \boldsymbol{d}_j) + \sum_{k \neq i, k \neq j}^{m} [\beta_{ijk} (\boldsymbol{d}_i + \boldsymbol{d}_j + \boldsymbol{d}_k) + \cdots] \right) \right) . \tag{23}$$

The physical meaning of (23) is explained as follows: In the magnetostatic case, for instance, one current dipole yields a pair of *north* and *south* magnetic poles on the measurement surface, which corresponds to the first term on the right hand side of (23). If the field consists of plural pairs of poles, the other terms should be taken into account in order. A similarly, in the electrostatic current flowing fields, the potential pattern is regarded as consisting of plural pairs of *positive* and *negative* poles caused by corresponding plural voltage dipoles. The problem can be reduced to determining the number of pole-pairs and their source positions.

Using the Cauchy–Schwarz relation in linear vector space [5], the first solution group in (10), i.e. the group of single pole-pairs, is given by

$$\frac{\boldsymbol{U}^{\mathrm{T}}\boldsymbol{d}_1}{|\boldsymbol{U}||\boldsymbol{d}_1|}, \quad \frac{\boldsymbol{U}^{\mathrm{T}}\boldsymbol{d}_2}{|\boldsymbol{U}||\boldsymbol{d}_2|}, \quad \ldots,$$
$$\frac{\boldsymbol{U}^{\mathrm{T}}\boldsymbol{d}_h}{|\boldsymbol{U}||\boldsymbol{d}_h|}, \quad \ldots, \quad \frac{\boldsymbol{U}^{\mathrm{T}}\boldsymbol{d}_m}{|\boldsymbol{U}||\boldsymbol{d}_m|}. \tag{24a}$$

The Cauchy–Schwarz relation of two vectors evaluates the pattern matching rate between the two vectors. This ratio does not depend on the source amplitude, so that the most dominant source position is uniquely determined by searching for the maximum term in (24a).

When the term $\boldsymbol{U}^{\mathrm{T}}\boldsymbol{d}_h/[|\boldsymbol{U}||\boldsymbol{d}_h|]$ in (24a) takes the maximum, the source located at point h is regarded as the first source yielding the field or potential pattern composed of a single pair of poles. In (24a), the estimated field pattern $\boldsymbol{d}_i$ $(i = 1, 2, \ldots, m)$ depends on the spatial angle of the voltage or current dipole, hence the position h should be determined by taking it into account.

Regarding the term $\boldsymbol{U}^{\mathrm{T}}\boldsymbol{d}_h/[|\boldsymbol{U}||\boldsymbol{d}_h|]$ as 1, the second solution group can be written as

$$\frac{\boldsymbol{U}^{\mathrm{T}}(\boldsymbol{d}_h+\boldsymbol{d}_1)}{|\boldsymbol{U}||\boldsymbol{d}_h+\boldsymbol{d}_1|}, \quad \frac{\boldsymbol{U}^{\mathrm{T}}(\boldsymbol{d}_h+\boldsymbol{d}_2)}{|\boldsymbol{U}||\boldsymbol{d}_h+\boldsymbol{d}_2|}, \quad \ldots, \quad 1,$$
$$\ldots, \quad \frac{\boldsymbol{U}^{\mathrm{T}}(\boldsymbol{d}_h+\boldsymbol{d}_m)}{|\boldsymbol{U}||\boldsymbol{d}_h+\boldsymbol{d}_m|}. \tag{24b}$$

for the source position estimation based on the field or potential pattern consisting of two pairs of poles.

A similar process is continued until the peak value of the sequential pattern matching rates, i.e. inner products, can be obtained. Thereby, the normalized solutions of (10) are approximately given by

$$\alpha_1[|\boldsymbol{d}_1|/|\boldsymbol{U}|] \simeq (1/m')[\boldsymbol{U}/|\boldsymbol{U}|]^{\mathrm{T}}\{[\boldsymbol{d}_1/|\boldsymbol{d}_1|] + [(\boldsymbol{d}_h+\boldsymbol{d}_1)/|\boldsymbol{d}_h+\boldsymbol{d}_1|]+\cdots\}, \tag{25a}$$

$$\alpha_2[|\boldsymbol{d}_2|/|\boldsymbol{U}|] \simeq (1/m')[\boldsymbol{U}/|\boldsymbol{U}|]^{\mathrm{T}}\{[\boldsymbol{d}_2/|\boldsymbol{d}_2|] + [(\boldsymbol{d}_h+\boldsymbol{d}_2)/|\boldsymbol{d}_h+\boldsymbol{d}_2|]+\cdots\}, \tag{25b}$$

$$\ldots,$$

$$\alpha_h[|\boldsymbol{d}_h|/|\boldsymbol{U}|] \simeq (1/m')\{[\boldsymbol{U}/|\boldsymbol{U}|]^{\mathrm{T}}[\boldsymbol{d}_h/|\boldsymbol{d}_h|] + 1 + 1 + \cdots\}, \tag{25c}$$

$$\ldots,$$

$$\alpha_m[|\boldsymbol{d}_m|/|\boldsymbol{U}|] \simeq (1/m')[\boldsymbol{U}/|\boldsymbol{U}|]^{\mathrm{T}}\{[\boldsymbol{d}_m/|\boldsymbol{d}_m|] + [(\boldsymbol{d}_h+\boldsymbol{d}_m)/|\boldsymbol{d}_h+\boldsymbol{d}_m|]+\cdots\}, \tag{25d}$$

where m' denotes the number of repeated processes similar to those of (24a) or (24b) and also corresponds to the number of pole-pairs of the field or potential pattern.

Regarding $\boldsymbol{d}_i$ $(i = 1, 2, \ldots, m)$ in (10) as basis vectors, each of the results in (25) can be interpreted as the spectrum corresponding to the basis vector. By analogy with the Fourier series, the Cauchy–Schwarz relation corresponds to the integration for obtaining spectrums. In the Fourier series:

$$f(t) = \sum_{i=-\infty}^{+\infty} C_i \exp(\mathrm{j}i\omega t), \tag{26a}$$

$$C_i = \frac{\omega}{2\pi}\int_{-\omega/\pi}^{\omega/\pi} f(t)\exp(-\mathrm{j}i\omega t)\,\mathrm{d}t. \tag{26b}$$

where $f(t)$ is an arbitrary periodic function, $\exp(\mathrm{j}i\omega t)$ $(i = -\infty, \ldots, -1, 0, 1, \ldots, +\infty)$ are sinusoidal basis functions, ω is a fundamental angular frequency, $\mathrm{j} = (-1)^{1/2}$ and C_i is the frequency spectrum corresponding to $\exp(\mathrm{j}i\omega t)$; the basis functions are orthogonal to each other. This means integrating the product of two different basis functions reduces to zero. Therefore, each spectrum can be uniquely determined by (26b). Equation (26b) corresponds to (25). How-

ever, our method has assumed that the angle between the basis vectors $\boldsymbol{d}_i$ and $\boldsymbol{d}_j$ $(i \neq j)$ is not orthogonal, so that (25) gives solution spectrums of (10) with some spreading bands, not the unique solution of (10) [7–11]. This corresponds to the Fourier transformation for a non-periodical function. In the Fourier transformation, obtained spectrums are continuous and form some spreading bands.

4. Examples

We have described the inverse problems in the electrostatic, magnetostatic and current flowing fields in a unified manner and shown that they can be formally reduced to solving the system equation (10). As examples, we demonstrate here the inverse problems concerning the magnetostatic fields. First, we apply our method to test examples in order to verify the validity of the method. Secondly, the method is applied to current distribution searching problem of human hearts from the MCG. Finally, the method is applied to current flow estimation in a human brain obtained from the MEG.

4.1. Uniqueness of solution patterns

As shown in fig. 1a, the first test example is that a straight current flows diagonally from the right upper hand corner to the left lower hand corner in a cubic region. The needle denotes the direction of the current flow. This current flow yields the magnetic field H_z normal to the top surface of the cube, as shown in fig. 1b. The z

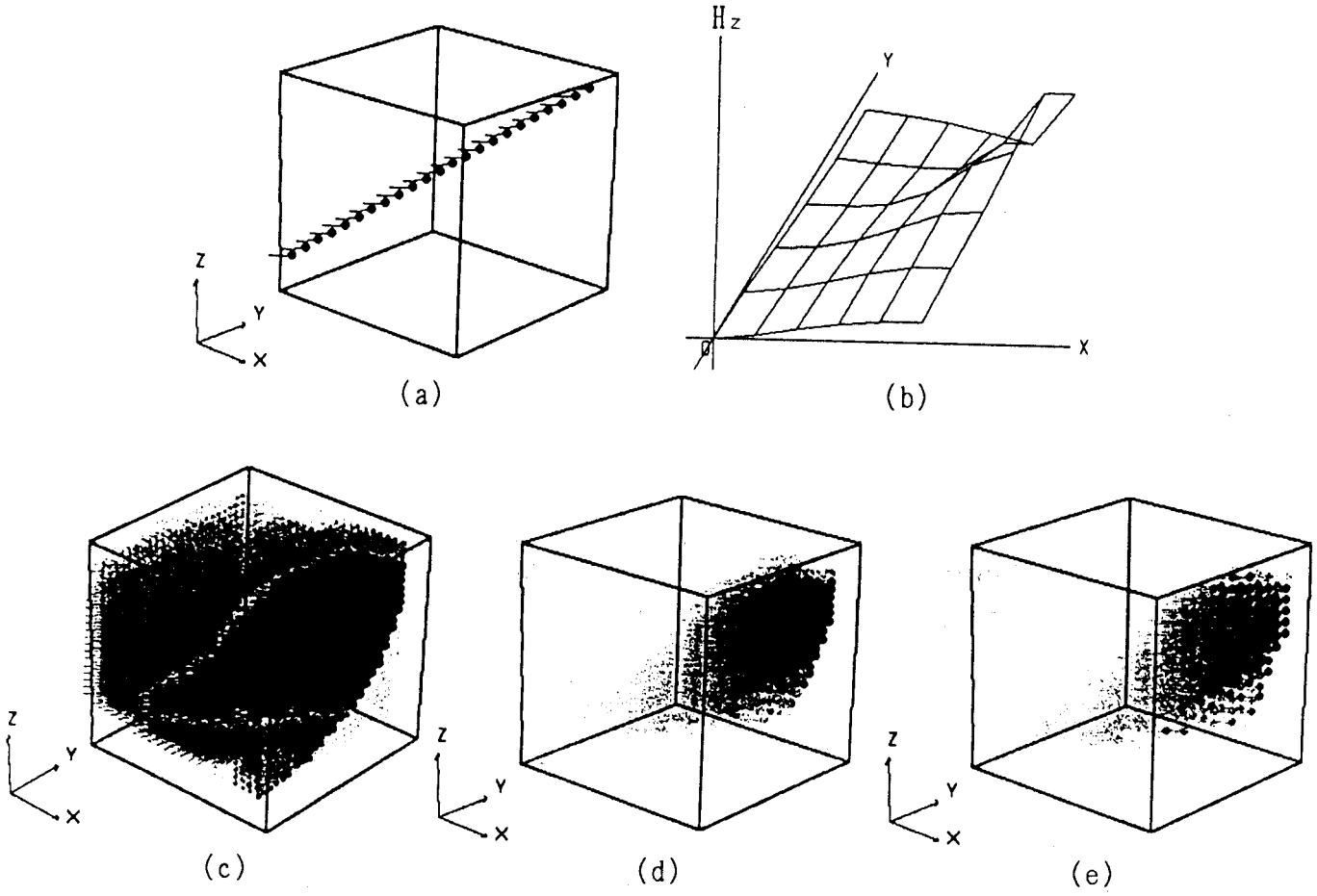

Fig. 1. Current flowing diagonally from the right upper hand corner to the left lower hand corner in a cubic region; (a) correct current distribution, (b) the magnetic field pattern H_z normal to the top surface due to the correct current distribution, (c) the estimated solution pattern ($m = 13\,225$ and 72 angle divisions), (d) the same result as (c) when showing top 10% for making it legible, (e) the estimated solution pattern showing its top 10% ($m = 5491$ and 72 angle divisions).

component of the current flow does not affect H_z because of the rotational relation (8b), so that it is possible to evaluate the x–y components of the current flow from the magnetic field H_z. Figure 1c shows the normalized solution pattern obtained by (25a)–(25d) with the field of fig. 1b, where the number of known or measured magnetic field intensities used in the calculation is $n = 6 \times 6 = 36$. In fig. 1c, the number of subdivisions in the cube and the angle resolution of the current dipoles on the x–y plane are $m = 13\,225$ and 5°, respectively, so that the total number of the unknowns in the system equation is $13\,225 \times 72 = 952\,200$. In order to make the result more legible, top 10% of the results obtained by (25a)–(25d) is shown in fig. 1d.

It is necessary to confirm the uniqueness of obtained solution patterns in inverse problems because we have infinite possibility for a solution of (10). This means a variety of solution patterns can give the same field pattern. If proposed algorithm give different solution patterns depending on system conditions, it is useless to analyze inverse problems. To verify the uniqueness of the solution patterns obtained by our method, the number of the subdivisions in the target volume, m has been changed. Figure 1e shows top 10% results of (25) obtained from the field of fig. 1b, where $n = 36$, $m = 5491$ and the number of the angle divisions for the current dipoles is 72. Comparing the results of figs. 1d and 1e suggests that the uniqueness of the solution patterns obtained by the SPM method [7–11] is verified.

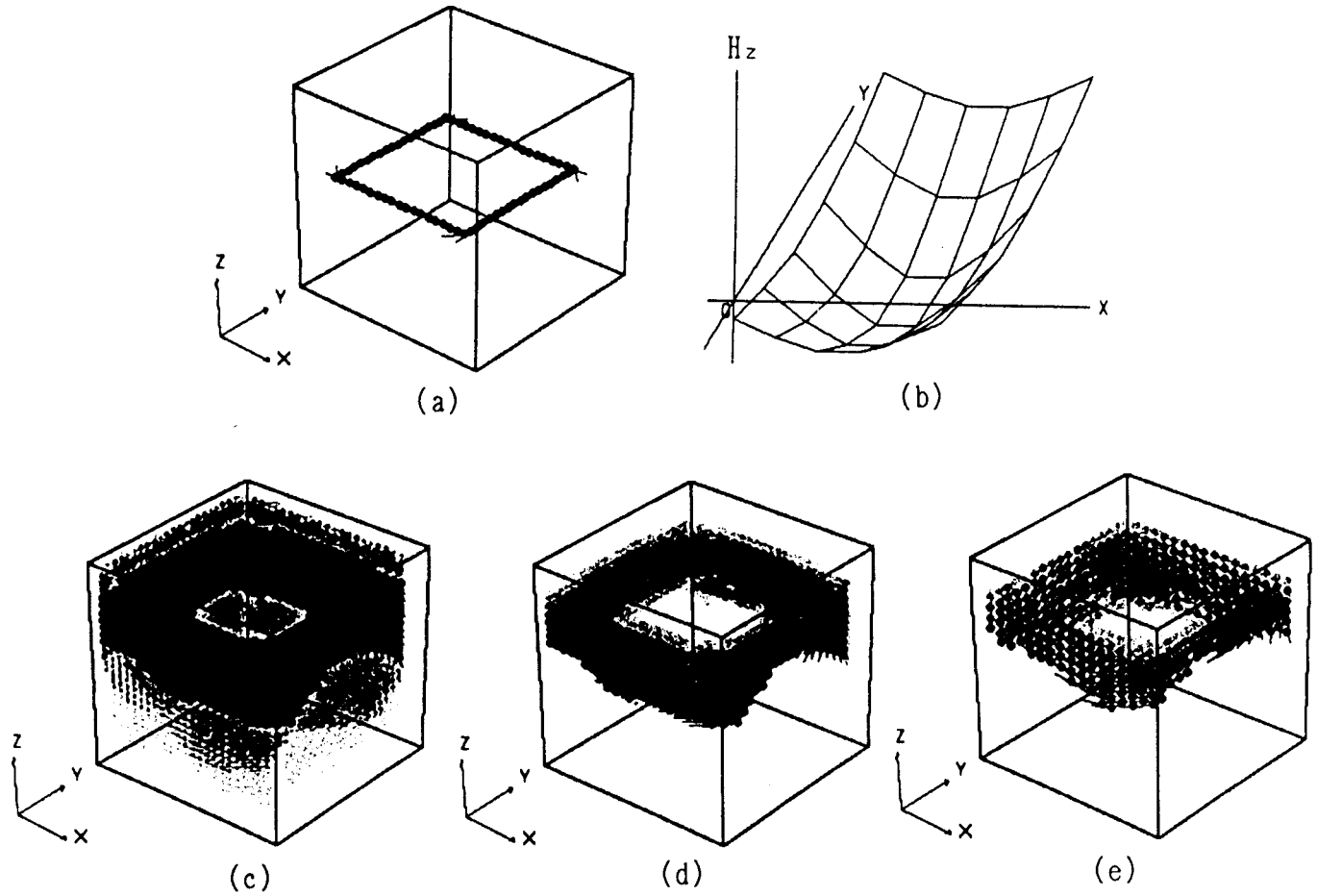

Fig. 2. Clockwise loop shape current distribution in parallel to the x–y plane; (a) correct current distribution, (b) the magnetic field pattern H_z normal to the top surface due to the correct current distribution, (c) the estimated solution pattern ($m = 13\,225$ and 72 angle divisions), (d) the same result as (c) when showing top 10% for making it legible, (e) the estimated solution pattern showing its top 10% ($m = 5491$ and 72 angle divisions).

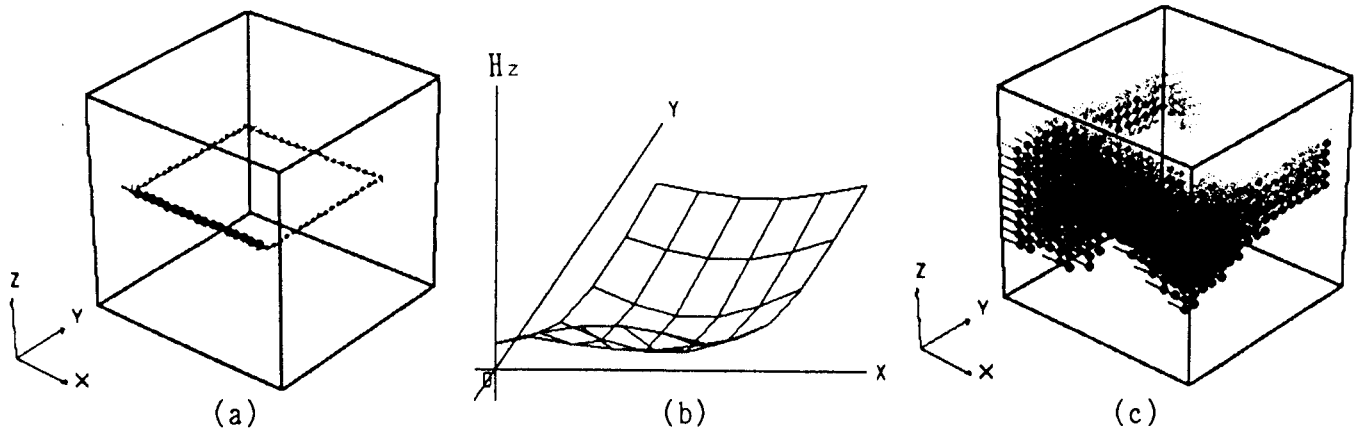

Fig. 3. Clockwise loop shape current distribution in parallel to the x–y plane, the current flowing in one side region is twice as large as those in the other three sides regions; (a) correct current distribution, (b) the magnetic field pattern H_z normal to the top surface due to the correct current distribution, (c) the estimated solution pattern showing its top 10% ($m = 5491$ and 72 angle divisions).

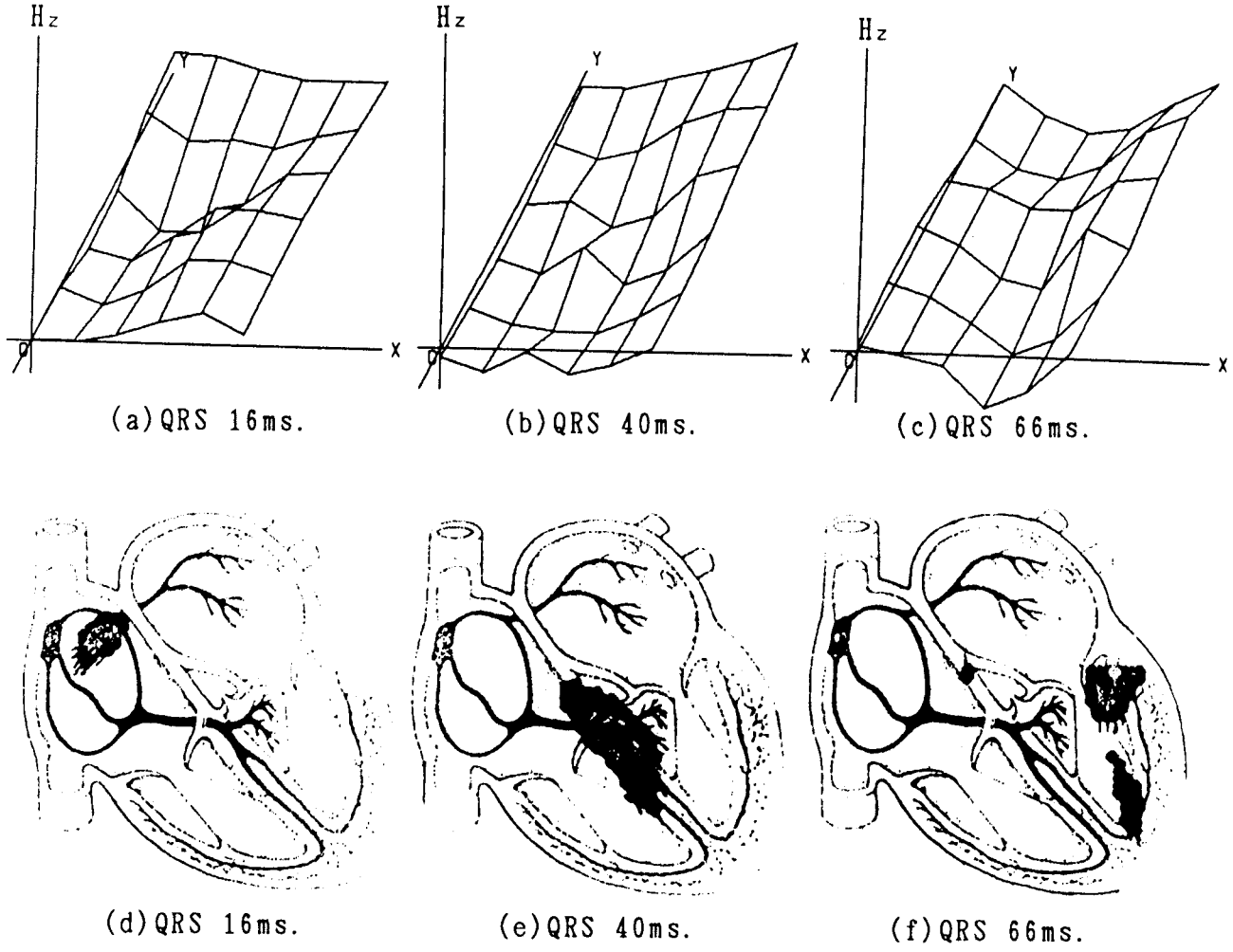

Fig. 4. The current distributions of a healthy human heart; (a)–(c) the MCGs, (d)–(f) the obtained solution patterns.

The second test example is a clockwise loop shape current flow case shown in fig. 2a. Figure 2b shows that the known or measured field pattern normal to the top surface of the cube has a concave shape. Figures 2c–2e show the results obtained from (25) with the field of fig. 2b, where the system conditions, i.e. n, m and the spatial angle division for the current dipoles, are the same as those in figs. 1c–1e, respectively. Even in a loop shape current flow case, the uniqueness of the solution patterns has been verified by comparing the results of figs. 2d and 2e with the correct current pattern shown in fig. 2a.

Practically obtained magnetic field is caused by the currents having different amplitudes in a target region. The final test example is to examine the effect of amplitude changes of currents. Figures 3a and 3b are a clockwise loop model current flow and its accompanying field pattern normal to the top surface of the cube, respectively. In fig. 3a, the amplitude of the current flowing in the negative x direction is twice as large as those of the other currents. Figure 3c shows the solution pattern obtained from the field of fig. 3b, where the system conditions are the same as those in fig. 1e. It is obvious from fig. 3c that the concentration rates of obtained spatial spectrums correspond to the amplitudes of the original currents. This result can be explained as follows: Basically, the Cauchy–Schwarz relation (24) gives source positions. However, the plural found source positions can be concentrated in the vicinity of the large amplitude current flowing region, even though the amplitudes of the computed spectrums are not proportional to the amplitudes of the original currents.

4.2. *Current distribution in hearts*

Depending on the heart operating conditions, the MCG exhibits the distinct patterns so that the MCG analysis is intensively studied for heart diagnosis [12]. Figures 4 and 5 show the MCGs [2] composed of the magnetic field H_z normal to the human chests and the estimated current distribution patterns on the x–y plane obtained by the SPM method [7–11], respectively. The estimated results in figs. 4 and 5 are showing the top 10% of the spectrums obtained from (25). And they have been obtained from a human healthy heart and the hearts of two patients with the Wolff–Parkinson–White (WPW) syndrome, respectively. Figures 4d, 4e and 4f show the current flows from the sino-atrial node to antioventicular node at QRS 16 ms, from the bundle of His conduction to the left as well as right bundles of QRS 40 ms and ending in the ramifying Purkinje fiber network at QRS 66 ms, respectively, The computed results of figs. 5c and 5d suggest that the defect positions of one patient is the Kent bundles and the other's is the James bundle with the WPW syndrome.

4.3. *Current distributions in a brain*

The unique solution pattern searching method is applied to the estimation of the current flows in a human brain. As a result, sequential current flows in a human brain reveal the functional behavior of the brain when the median nerve of the right wrist is stimulated electrically [13]. The electrically stimulated pulse is a square wave having the period 0.5 s.

Figures 6a–6c show the MEGs measured on the surface over the left brain of a healthy 22-year-old man at 70 ms, 100 ms and 150 ms, respectively, after the stimulation [13]. The MEGs are composed of the magnetic field intensities H_z normal to the measurement surface, therefore, the estimated currents should be distributed in parallel to the surface. Figurers 6d–6f show the top 10% estimated current distributions obtained by (25) at 70 ms, 100 ms and 150 ms, respectively.

At 70 ms after the pulse impressed at the median nerve of the right wrist, fig. 6d shows that the signal reaches the brain via a vertebra. At 100 ms, the signal stays at the hand sensory cortex but strong recognition and memorization are carried out, as shown in fig. 6e. At 150 ms, the signal at the brainstem becomes the strongest, as shown in fig. 6f.

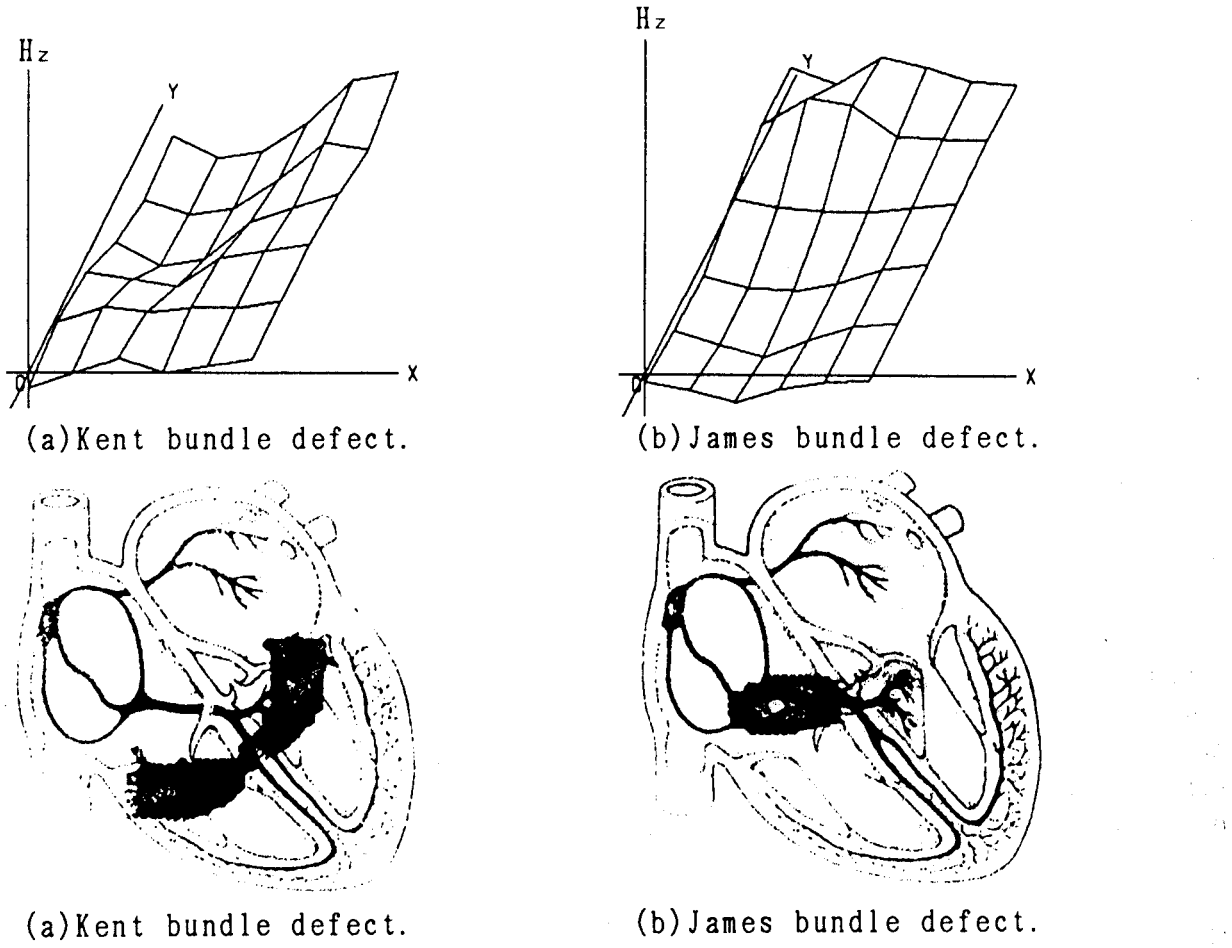

Fig. 5. The current distributions in human hearts of the WPW syndrome; (a)–(b) the MCGs at QRS 30 ms, (c)–(d) the obtained solution patterns.

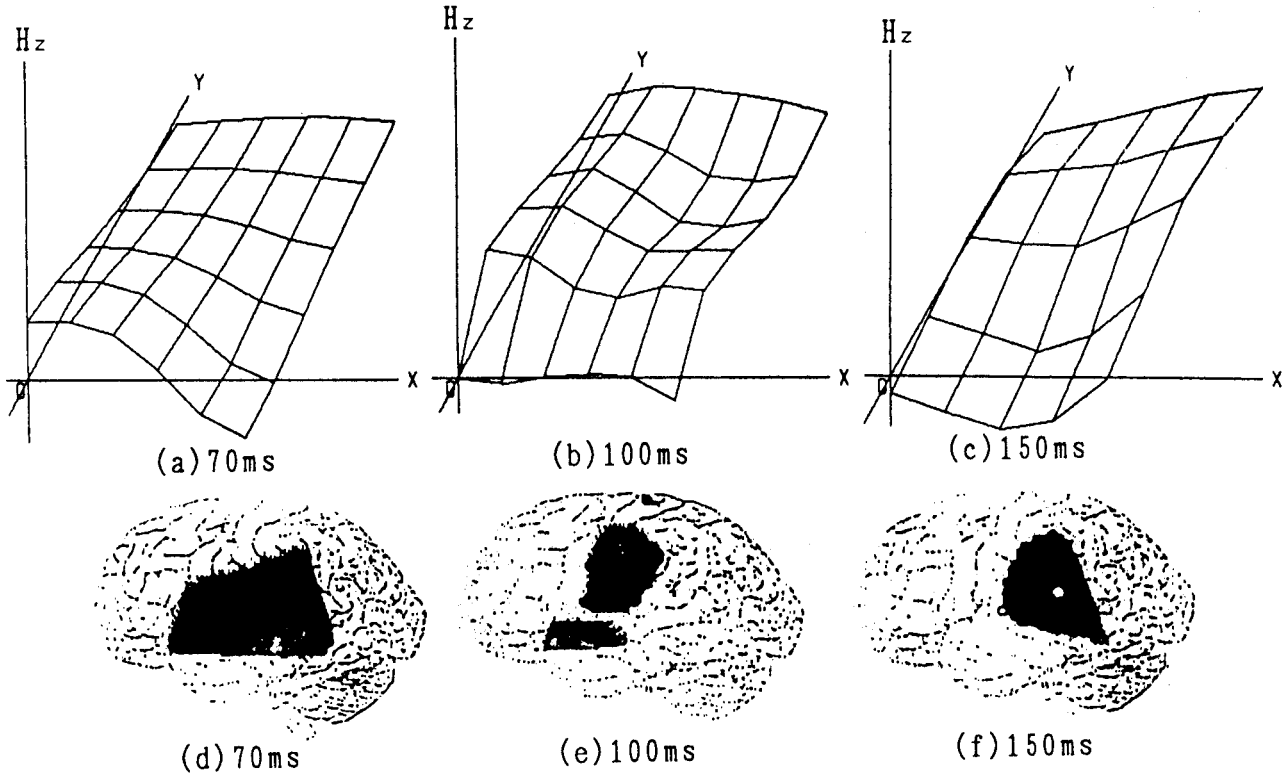

Fig. 6. The normalized current distributions in a human brain when the median nerve of the right wrist is stimulated electrically; (a)–(c) the MEGs, (d)–(f) the obtained solution patterns.

5. Conclusion

As shown above, we have tried a unified approach to the open boundary inverse problems of electromagnetic fields. As a result, we have succeeded in deriving a general form of governing equations as well as system equations for the inverse problems. Further, we have proposed the unique solution pattern searching method to analyze the inverse problem with the system equation where the number of equations is less than the number of the unknowns. The solution pattern, not the exact solution, has been successfully evaluated, also the uniqueness of the solution patterns has been verified by the test examples.

Finally, we have applied the method to the medical diagnosis. As a result, the positions of defect in the human heart exhibiting the WPW syndrome have been identified by the local magnetic field measurements, and the proposed method makes it possible to investigate the human brain's functional operations.

References

[1] G. Anger, Inverse Problems in Differential Equations (Plenum Press, New York, 1990).

[2] K. Watanabe, A. Takeuchi, M. Katayama, Y. Fukuda, M. Nomura, M. Sumi, M. Murakami, Y. Nakaya and H. Mori, Analysis of activation sequence by isomagnetic and vector arrow maps, in: Biomagnetism '87, Eds. K. Atsumi et al. (Tokyo Denki University Press, Japan, 1988) pp. 346–349.

[3] T. Katila, Functional localization studies in magnetocardiography, J. Appl. Electromagn. Mater. 1 (1990) 179–187.

[4] Y. Uchikawa and M. Kotani, Tracing of the equivalent source localization in the brain to somatosensory evoked magnetic field equivalent current dipole technique, T. IEE Japan 112A (1992) 127–132.

[5] G. Strang, Linear Algebra and its Applications, (Academic Press, New York, 1976).

[6] R.D. Paola, J.P. Brazin, F. Aubry, A. Aurengo, F. Cavailloloes, J.Y. Herry and E. Kahn, Handling of dynamnic sequences in nuclear medicine, IEEE Trans. Nucl. Sci. NS-29 (1982) 1310–1321.

[7] Y. Saito, E. Itagaki and S. Hayano, A formulation of the inverse problems in magnetostatic fields and its application to a source position searching of the human eye fields, J. Appl. Phys. 67 (1990) 5830–5832.

[8] H. Saotome, K. Kitsuta, S. Hayano and Y. Saito, Inverse problems in biomagnetic fields, T. IEE Japan 112 A (1992) 279–286.

[9] H. Saotome, K. Kitsuta, S. Hayano and Y. Saito, An estimation of current distribution in biological system by the sampled pattern matching method, T. IEE Japan 113C, No. 1 (1993) 101–108.

[10] H. Saotome, K. Kitsuta, S. Hayano and Y. Saito, A neural behavior estimation by the generalized correlative analysis, IEEE Trans. Magn. (March, 1993), in press.

[11] H. Saotome, T. Doi, S. Hayano and Y. Saito, Crack identification in metallic materials, IEEE Trans. Magn. (March, 1983), in press.

[12] M. Nomura, K. Fujino, M. Katayama, A. Takeuchi, Y. Fukuda, M. Sumi, M. Murakami, Y. Nakaya and H. Mori, Analysis of the T wave of the magnetocardiogram in patients with essetnial hypertension by means of isomagnetic and vector arrow maps, J. Electrocardiol. 21 (1988) 174–182.

[13] Y. Uchikawa, T. Hasegawa, K. Aihara and M. Kotani, Measurement of somatosensory evoked magnetic fields induced by electric simulation, J. Japan Appl. Magn. 13 (1989) 508–512.